arXiv:1407.5657v2 [cond-mat.supr-con] 10 Jul 2015

Large electron-phonon interactions from FeSe phonons in a monolayer

Sinisa Coh,* Marvin L. Cohen, and Steven G. Louie
Department of Physics, University of California at Berkeley and Materials Sciences Division, Lawrence Berkeley National Laboratory, Berkeley, California 94720, USA
(Dated: July 14, 2015)

We show that electron-phonon coupling can induce strong electron pairing in an FeSe monolayer on a $SrTiO_3$ substrate (experimental indications for superconducting T_c are between 65 and 109 K). The role of the $SrTiO_3$ substrate in increasing the coupling is two-fold. First, the interaction of the FeSe and TiO_2 terminated face of $SrTiO_3$ prevents the FeSe monolayer from undergoing a shear-type (orthorhombic, nematic) structural phase transition. Second, the substrate allows an anti-ferromagnetic ground state of FeSe which opens electron-phonon coupling channels within the monolayer that are prevented by symmetry in the non-magnetic phase. The spectral function for the electron-phonon coupling (α^2F) in our calculations agrees well with inelastic tunneling data.

PACS numbers: 74.78.Na,74.20.Pq

Small variations of external perturbations can result in the favoring of one of a range of competing structural, electronic, and magnetic ground states for FeSe. In particular, the superconducting transition temperature in FeSe is reputed to vary from almost 0 K when slightly Fe doped [1] to 65 K when placed in a monolayer form on a $SrTiO_3$ substrate [2–5], and transport measurements from a recent work [6] indicate an even larger T_c, close to 109 K. Although FeSe has a simpler structure to the other iron-based superconductors it resembles components of their structure, and there is the possibility that the mechanism responsible for high temperature superconductivity in monolayer FeSe may extend to other iron-based compounds.

Early calculations (Refs. [7, 8]) based on density functional theory (DFT) estimated electron-phonon coupling in the iron-based superconductors to be at least 5-6 times too small to explain the transition temperatures found experimentally. Therefore, a large part of the theoretical and the experimental [9–11] work on iron-based superconductors in the literature focused on alternative electron pairing mechanisms such as those associated with magnetic fluctuations. In this letter we suggest that the early first-principle calculations may have underestimated the electron-phonon coupling in FeSe, and we conclude that conventional electron-phonon coupling may be strong enough to contribute significantly to the electron pairing in an FeSe monolayer on $SrTiO_3$ and perhaps other iron-based superconductors.

We focus here on an FeSe monolayer on a TiO_2 terminated $SrTiO_3$ substrate. We show that the interaction between the substrate and the FeSe monolayer leads to a high phonon-mediated superconducting T_c by providing a *structural template* which holds FeSe near its structural and magnetic phase transitions. When this structural template is not present (as in bulk FeSe or a monolayer of FeSe on a weakly interacting substrate) the system condenses to a different ground state (orthorhombic and non-magnetic) with a reduced electron-phonon coupling.

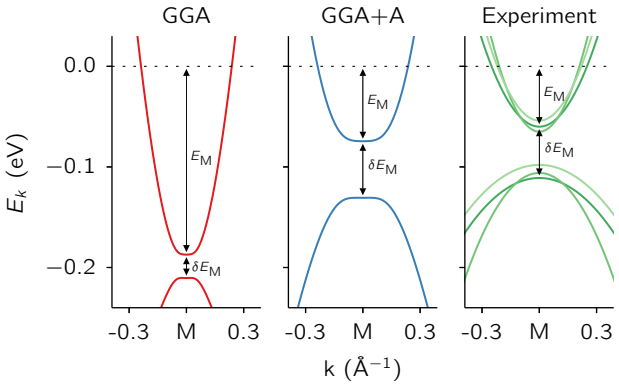

FIG. 1. Electronic band structure near the M point (full band structure is shown in the supplement [23]) of monolayer FeSe on $SrTiO_3$ in GGA (red), GGA+A with $A = A_c$ (blue), and experimental results. We fit the different experimental data to a parabola (light [3], medium [4], and dark green [5]).

Among the many possible ground states of FeSe, calculations based on a semi-local density approximation (GGA) to the DFT select a ground state inconsistent with structural [12], electronic [13–16], and magnetic [12, 17] measurements. While the shortcomings of standard GGA bands for transition metals (such as Fe) can often be corrected by semi-empirically including a Hubbard or a Hund interaction (as in the GGA+U method, [18]), this is not the case for FeSe.[19] Higher levels of theory, such as GW or DMFT in Refs. [20, 21], can correctly reproduce most electronic properties of bulk FeSe; however, calculation of the electron-phonon coupling with these methods relies on a simplified deformation potential approximation, as in Ref. [22] since electron-phonon coupling matrix elements are difficult to obtain.

Here we show that making the potential on the iron atoms slightly more repulsive for electrons renormalizes the bands near the Fermi level and selects a ground state

TABLE I. A comparison of the magnetic moment on the iron atom (μ), shear angle α (measured between the primitive unit cell vectors a and b), top of the Γ band (E_Γ) and bottom of the M band (occupied bandwidth, E_M) relative to the Fermi level, and the band splitting at the M point (δE_M) in GGA, GGA+A using $A = A_c$, and from experiments (Refs. [1, 3–5, 17]). Parameter A is tuned to $A = A_c$ so that occupied bandwidth of the M-point electron pocket (E_M) agrees with experimental data. However, using $A = A_c$ significantly improves other properties of FeSe as well.

	Bulk		Monolayer on $SrTiO_3$			
	μ[a]	α[b]	μ	E_Γ	E_M	δE_M
	(μ_B)	(°)	(μ_B)	(eV)	(eV)	(eV)
GGA	2.4	90	2.6	0.66	0.19	0.02
GGA+A (A_c)	0	89.96	1.8	0.17	0.07	0.06
Experiment	0	89.7	[c]	0.08	0.06	0.05

[a] Using experimental crystal structure.
[b] Fully relaxed with the van der Waals correction from Ref. [24].
[c] Unknown.

of FeSe consistent with most experimental data. More specifically, in this method (GGA+A), we empirically[25] replace the potential $V_{GGA}(\mathbf{r})$ within the semi-local density approximation (GGA) with

$$V_{GGA}(\mathbf{r}) + A\sum_i f(|\mathbf{r} - \mathbf{r}_i|). \quad (1)$$

The idea here is to mitigate empirically the fact that the GGA exchange-correlation potential is not the self energy without the second term in Eq. 1. We find that the detailed form of the dimensionless function $f(r) > 0$ is irrelevant for the computed physical properties of FeSe, as long as $f(r)$ is peaked on the Fe atom (placed at $\mathbf{r}_i$) and the extent of $f(r)$ is comparable with the size of the iron atom d-orbital. [26] Next, for a fixed $f(r)$, we tune the parameter A from 0 up to A_c (> 0) until [27] one of the properties of FeSe (here, occupied bandwidth of the M-point electron pocket) agrees with experimental data (compare blue and green curves in Fig. 1). Remarkably, using $A = A_c$ improves other salient properties of FeSe as well. For example, the gap (δE_M in Table I) at the bottom of the M pocket, and the energy of the Γ band just below the Fermi level are improved in the GGA+A, as well as the peak positions in the density of states at 4 and 6 eV below the Fermi level. [28] Magnetic properties are improved as well. Using the experimental crystal structure from Ref. [29] in both cases, the GGA+A predicts *bulk* FeSe to be nonmagnetic as in experiment, while GGA predicts large antiferromagnetically aligned magnetic moments μ on the iron atoms (favored by 0.5 eV per two Fe atoms over the non-magnetic ground state). Finally, the crystal structure is improved in the GGA+A case. A slight shear present in the experimental structure as in Ref. [1] ($\alpha < 90°$) remains in the GGA+A approach

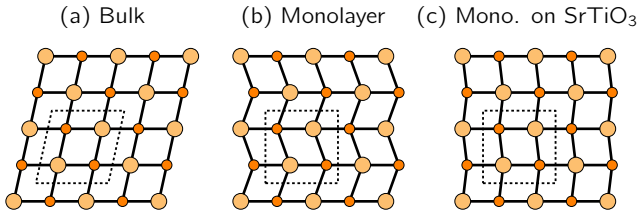

FIG. 2. Exaggerated structural distortions in FeSe bulk, an epitaxially constrained monolayer, and a monolayer on $SrTiO_3$. Small circles are Fe atoms and large circles are Se atoms. Primitive unit cell is shown with a dashed gray line.

after the structural relaxation, while it disappears in the GGA calculations ($\alpha = 90°$).

In these and subsequent calculations we fixed the doping of FeSe monolayer to the level of 0.09 electrons per one Fe atom (as found in ARPES experiments). In the experiment, this doping likely occurs due to presence of oxygen vacancies in the $SrTiO_3$ substrate.

Our focus here is on the electron-phonon coupling and superconductivity in monolayer FeSe. The underlying origin of the success of the GGA+A is an interesting open question and is left for future studies. We only note here two points in favor of GGA+A. First, portion of the electron self-energy $\Sigma(\mathbf{r}, \mathbf{r}', E)$ that is missing in the semi-local density approximation is typically large only when $|\mathbf{r}-\mathbf{r}'|$ is comparable to the bond length,[30] just as for the case of the form of $f(r)$. Second, agreement between GGA+A and experiment is improved not only in monolayer FeSe studied here, but also in bulk $KCuF_3$, $LaNiO_3$, $(La,Sr)_2CuO_4$, $SrTiO_3$ (see supplement[23]), and $(Ba,K)Fe_2As_2$.[31]

Equipped with a better FeSe band structure and ground state than obtained from a standard GGA calculation, we are now in a position to compute the electron-phonon coupling strength in the FeSe monolayer. First we discuss the crystal structure of FeSe used in the electron-phonon calculation. Bulk FeSe consists of stacked, weakly interacting, layers of FeSe. Below 90 K these layers are observed to be slightly sheared as shown in Fig. 2a and discussed in Ref. [1] (shear is also present in GGA+A calculation, but not in GGA). This shear (nematic) distortion is conventionally described as primitive-tetragonal to base-centered-orthorhombic structural phase transition.

Since the FeSe layers in bulk are only weakly interacting, we expect that the tendency towards a shear distortion will be present even in an *isolated* single layer of FeSe. This is indeed what we find in the case of monolayer FeSe. Even if we epitaxially constrain the isolated monolayer FeSe unit cell to a cubic $SrTiO_3$ lattice, it still undergoes a local shear-like structural transition shown in Fig. 2b (again, only in GGA+A, not in GGA).

However, once FeSe is placed on a TiO_2 terminated $SrTiO_3$ substrate, we find that the interaction of Ti and Se atoms together with the epitaxial strain is able to stabilize FeSe to a nearly square arrangement (see Fig. 2c and supplement[23]). A small remnant of the structural distortion present in FeSe is responsible for the electronic gap ($\delta E_{\rm M}$) at the M point shown in Fig. 1 and in Table I. (An additional smaller component of the gap results from a built-in electric field between FeSe and $SrTiO_3$, as discussed in Ref. [19].) In addition, in the FeSe *monolayer* on $SrTiO_3$, an antiferromagnetic checkerboard ground state is preferred by 0.11 eV (per unit cell with two Fe atoms) within GGA+A over the non-magnetic one, despite the fact that the opposite is the case for *bulk* FeSe.

The main effect of the $SrTiO_3$ on the FeSe is the structural stabilization described above of a non-sheared and antiferromagnetic ground state. Selection of this ground state then affects the electronic and magnetic properties of FeSe, but only indirectly through the fact that FeSe is in this particular state. The direct effect of the $SrTiO_3$ on the electronic structure of an FeSe monolayer near the Fermi level is negligible. For example, relaxing the structure of FeSe on $SrTiO_3$ and then removing $SrTiO_3$ atoms from the calculation does not affect the electronic structure near the Fermi level (see Fig. 1 in the supplement [23]). Therefore to speed up the calculation of the electron-phonon coupling, we perform calculations on an isolated FeSe layer, without explicitly including $SrTiO_3$. To avoid the shear instability in the FeSe monolayer from removing of $SrTiO_3$, we reduce the value of parameter A in Eq. 1 from $A_{\rm c}$ to $0.9A_{\rm c}$ and confirm that the electron-phonon matrix elements are not affected by this simplification by carrying out full calculation (see Table. 1 in the supplement[23]).

We use state-of-the-art Wannier interpolation technique from Ref. [32] and the Quantum-Espresso package described in Ref. [33] to calculate the electron-phonon coupling in the FeSe monolayer with a very fine grid in the Brillouin zone (40×40). We obtained the superconducting transition temperature $T_{\rm c}$ by solving the Eliashberg equation [34, 35] as described in Ref. [36]. Figure 3 shows the calculated Eliashberg spectral function $\alpha^2F(\omega)$ of the FeSe monolayer. We focus our analysis on two groups of phonons for which the electron-phonon coupling is the largest. The first group of phonons (labeled 1 in Fig. 3) corresponds to phonons with frequency close to 10 meV, and the second group (labeled 2) to phonons with 20 meV (in GGA those frequencies are 15 and 25 meV, respectively).

While phonons 1 contribute to about two-thirds of the total electron-phonon coupling strength λ, they contribute to about half of the integrated $\alpha^2F(\omega)$ spectral function (since they have a lower frequency).

The atomic displacement character of the two groups of phonons is different. Phonons 1 correspond to a branch of phonons that involve transverse, mostly in-plane displacements of atoms (these phonons cause bulk FeSe to undergo a shear phase transition), while phonons 2 correspond to an out-of-plane transverse displacement of Fe atoms. Furthermore, phonons 1 and 2 couple different parts of the electron Fermi surface at M. Phonons 1 couple mostly at parts of the reciprocal space where the Fermi surface (electron M pocket) crosses the M–Γ line and the least where it crosses the M–X line. The opposite is true for phonons 2. However, since both phonons contribute about equally to α^2F the total electron-phonon coupling (1 and 2 taken together) is nearly constant on the entire M pocket Fermi surface.

Hence the importance of the $SrTiO_3$ substrate for increasing the superconducting transition temperature within the phonon mechanism in FeSe is two-fold. First, it prevents phonons 1 from becoming unstable and induce a structural phase transition (as in bulk FeSe). Second, $SrTiO_3$ keeps FeSe in the checkerboard magnetic phase which allows coupling of phonons from groups 1 and 2. In the non-magnetic case, the coupling of these phonons is zero by symmetry.[37] Calculations in Refs. [38, 39] also found a significantly smaller electron-phonon coupling in the non-magnetic phase than in the magnetic phase. We also note that at this time, there is no direct experimental measurement of magnetic order in FeSe monolayer on

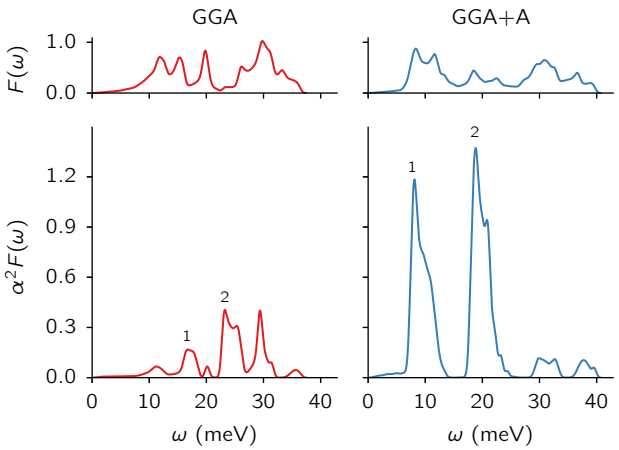

FIG. 3. Electron-phonon coupling $\alpha^2F(\omega)$ and phonon density of states $F(\omega)$ (in meV^{-1}) in GGA and GGA+A (using $A = 0.9A_{\rm c}$).

TABLE II. Electron-phonon coupling (λ), density of states (DOS), and average phonon frequencies in GGA and conservative estimates in GGA+A.

	λ	DOS (eV^{-1})	$\sqrt{\langle\omega^2\rangle}$ (K)
GGA	0.3	1.0	252
GGA+A	1.6	1.8	171

$SrTiO_3$. However, the measured ARPES band structure is most closely resembled to that of the band structure of FeSe with an antiferromagnetic checkerboard order, both in our GGA+A calculation and in previous work.[19, 40] Nevertheless, it is possible that the true ground state of FeSe monolayer consists of fluctuating antiferromagnetic moments on iron atoms. Treatment of electron-phonon coupling in such a state from first-principles goes well beyond the scope of this work.

Comparing $\alpha^2F(\omega)$ in GGA and GGA+A (Fig. 3), we find two reasons for an increased coupling in GGA+A. First, preference for a shear distortion in GGA+A increases the electron-phonon matrix elements of phonons 1 (see Fig. 3 in the supplement [23]). Second, the bottom of the electron M pocket E_M is closer to the Fermi level in GGA+A than in the GGA. Therefore, owing to this band renormalization (narrowing of the occupied bandwidth), the density of states at the Fermi level in GGA+A is larger than in GGA (see Table II here and Fig. 3 in the supplement [23]). Since λ is proportional to the density of states, it is therefore increased in GGA+A.

However, as discussed earlier, we calculated the electron-phonon coupling λ within GGA+A with a reduced value of parameter A from Eq. 1. Taking into account calculated density of states (1.5 eV^{-1}) with $A = 0.9A_c$ and $A = A_c$ (1.8 eV^{-1}) we conservatively estimate that the value of λ at $A = A_c$ is $\lambda = 1.6$. Next we use the Eliashberg theory and obtain a conservative estimate of the superconducting transition temperature T_c of 26 K (with $\mu^* = 0.0$) and 21 K (with $\mu^* = 0.1$). This estimate is significantly closer to experiment than a standard GGA result (0.1–1.5 K).

This range of estimated transition temperatures (21–26 K) is close to the value found across the families of bulk iron-based superconductors. Now we discuss possible reasons for an even larger T_c in the case of an FeSe monolayer on $SrTiO_3$ (65–109 K).

When λ is large, transition temperature is proportional to [41]

$$T_c \sim \overline{\omega}\lambda^{0.5}. \quad (2)$$

Here $\overline{\omega}$ is the averaged phonon frequency and λ is the Brillouin zone averaged electron-phonon coupling strength. Therefore one possibility to get larger T_c is to further increase λ. It is at least plausible that this could happen for phonons 1, since their contribution to λ is increased when FeSe is approaching the shear-like structural phase transition.

The second possibility is to increase the average frequency $\overline{\omega}$ by pairing electrons with high frequency modes (phonons or some other bosons) in addition to phonons 1 and 2. One possibility are magnetic fluctuations [8]. The role of magnetism for superconductivity in FeSe is additionally enriched by the fact that, in the nonmagnetic phase, certain electron-phonon interaction channels are forbidden by symmetry. In addition, structural and magnetic order parameters are strongly coupled in FeSe. For example, bulk orthorhombic FeSe prefers a non-magnetic state, while a cubic FeSe monolayer on $SrTiO_3$ prefers an antiferromagnetic state.

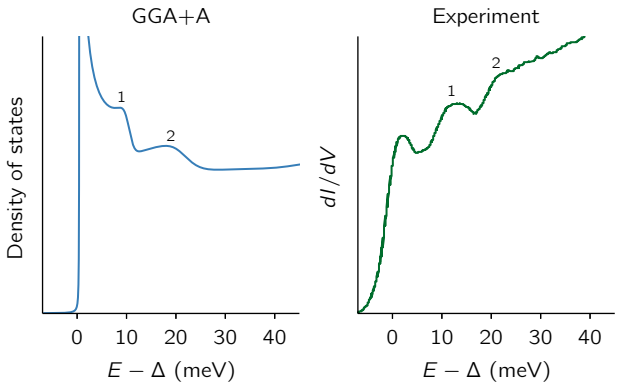

FIG. 4. The density of states within the Eliashberg theory calculated using GGA+A and the STM measurement from Ref. [42]. The energy is measured relative to the superconducting gap Δ.

Another tempting possibility suggested in Ref. [3] is to pair FeSe electrons to a high-frequency (80 meV) phonon in the $SrTiO_3$ substrate. This coupling was experimentally determined to be large near the origin of the phonon Brillouin zone ($q \sim 0$). Adding experimentally estimated values of the electron-phonon coupling from Ref. [3] to our calculated $\alpha^2F(\omega)$ increases the estimated superconducting transition temperature to 47 K (assuming $\mu^* = 0.1$), even closer to the experimentally determined value (65–109 K).

In closing, we note that the experimentally inferred superconducting T_c is nearly the same for an FeSe monolayer on TiO_2 terminated $SrTiO_3$ [2, 6], $BaTiO_3$ [43], as well as 2% strained $SrTiO_3$ [44]. This observation is consistent with our structural stabilization mechanism since in all three cases interaction between Ti atoms in the TiO_2 layer and Se atoms in FeSe is likely the same. However, when a FeSe monolayer is placed on a substrate with a different bonding environment, such as SiC in Ref. [45–47] the superconducting T_c is only 2–9 K. Another indication for the importance of structural stabilization comes from Ref. [1]. This study found that bulk FeSe doped with only 2% of iron stays tetragonal (non-sheared) even well below 90 K. This loss of preference for shear is accompanied with loss of superconductivity ($T_c < 0.5$ K), again consistent with our finding that keeping FeSe close to a shear (orthorhombic, nematic) structural phase transition increases the electron-phonon coupling strength. Another indication of contribution from electron-phonon mechanism is described in Ref. [48] on iron isotope effect measurement.

Finally, our calculation is consistent with the inelastic scanning tunneling microscope (STM) measurements from Ref. [42] in two respects. First, the superconducting gap in the STM measurements (as well as in ARPES in Refs. [4, 44]) is node-less, just as is our calculated electron-phonon coupling being nearly constant around the M pocket. Second, both our calculation and the STM measurements find two peaks in the density of states above the superconducting gap Δ (see Fig. 4). One of these peaks is at 10 meV and another at 20 meV above the gap. As shown in Ref. [49], features in the tunneling spectrum above the gap can be associated with α^2F. Therefore, we tentatively assign the two peaks found in the STM measurements to the strongly electron-phonon coupled modes 1 and 2 discussed earlier in the text.

This research was supported by the Theory Program at the Lawrence Berkeley National Lab through the Office of Basic Energy Sciences, U.S. Department of Energy under Contract No. DE-AC02-05CH11231 which provided for the electron-phonon calculation; and by the National Science Foundation under Grant No. DMR10-1006184 which provided for the structural and magnetic study. This research used resources of the National Energy Research Scientific Computing Center, which is supported by the Office of Science of the U.S. Department of Energy.

* sinisacoh@gmail.com

[1] T. M. McQueen, A. J. Williams, P. W. Stephens, J. Tao, Y. Zhu, V. Ksenofontov, F. Casper, C. Felser, and R. J. Cava, Phys. Rev. Lett. **103**, 057002 (2009).
[2] W. Qing-Yan *et al.*, Chin. Phys. Lett. **29**, 037402 (2012).
[3] J. J. Lee *et al.*, Nature **515**, 245 (2014).
[4] D. Liu *et al.*, Nat Commun **3**, 931 (2012).
[5] S. He *et al.*, Nat Mater **12**, 605 (2013).
[6] J.-F. Ge, Z.-L. Liu, C. Liu, C.-L. Gao, D. Qian, Q.-K. Xue, Y. Liu, and J.-F. Jia, Nat. Mater. **14**, 285 (2014).
[7] L. Boeri, O. V. Dolgov, and A. A. Golubov, Phys. Rev. Lett. **101**, 026403 (2008).
[8] I. I. Mazin, D. J. Singh, M. D. Johannes, and M. H. Du, Phys. Rev. Lett. **101**, 057003 (2008).
[9] T. Imai, K. Ahilan, F. L. Ning, T. M. McQueen, and R. J. Cava, Phys. Rev. Lett. **102**, 177005 (2009).
[10] M. D. Lumsden, A. D. Christianson, E. Goremychkin, S. E. Nagler, H. Mook, M. B. Stone, D. L. Abernathy, T. Guidi, G. J. MacDougall, C. de la Cruz, *et al.*, Nature physics **6**, 182 (2010).
[11] T. Hanaguri, S. Niitaka, K. Kuroki, and H. Takagi, Science **328**, 474 (2010).
[12] A. Subedi, L. Zhang, D. J. Singh, and M. H. Du, Phys. Rev. B **78**, 134514 (2008).
[13] K. Nakayama, T. Sato, P. Richard, T. Kawahara, Y. Sekiba, T. Qian, G. F. Chen, J. L. Luo, N. L. Wang, H. Ding, and T. Takahashi, Phys. Rev. Lett. **105**, 197001 (2010).
[14] A. Tamai *et al.*, Phys. Rev. Lett. **104**, 097002 (2010).
[15] F. Chen *et al.*, Phys. Rev. B **81**, 014526 (2010).
[16] J. Maletz *et al.*, Phys. Rev. B **89**, 220506 (2014).
[17] S. Li *et al.*, Phys. Rev. B **79**, 054503 (2009).
[18] A. I. Liechtenstein, V. I. Anisimov, and J. Zaanen, Phys. Rev. B **52**, R5467 (1995).
[19] F. Zheng, Z. Wang, W. Kang, and P. Zhang, Sci. Rep. **3**, 2213 (2013).
[20] Z. P. Yin, K. Haule, and G. Kotliar, Nat Mater **10**, 932 (2011).
[21] J. M. Tomczak, M. van Schilfgaarde, and G. Kotliar, Phys. Rev. Lett. **109**, 237010 (2012).
[22] S. Mandal, R. E. Cohen, and K. Haule, Phys. Rev. B **89**, 220502 (2014).
[23] See end of this PDF document for supplemental material.
[24] S. Grimme, J. Comput. Chem. **27**, 1787 (2006).
[25] This approach is similar in spirit to the empirical pseudopotential method from Ref. [50] and the semi-empirical method from Ref. [51].
[26] For example, we tried $f(r) \sim r^n \exp(-Br^m)$ with several choices of $0 < n < 4$, $1 < m < 4$, and B all giving similar results.
[27] We give in the supplement[23] the numerical value of $A_c f(r)$, a list of all parameters used in the calculations, and a figure showing the dependence of several physical properties of FeSe monolayer on the value of A.
[28] In GW calculations from Ref. [21] these same peaks near 4 and 6 eV were found to agree well with the experiment.
[29] D. Phelan, J. N. Millican, E. L. Thomas, J. B. Leão, Y. Qiu, and R. Paul, Phys. Rev. B **79**, 014519 (2009).
[30] M. S. Hybertsen and S. G. Louie, Phys. Rev. B **34**, 5390 (1986).
[31] H. Oh, S. Coh, and M. L. Cohen, arXiv:1502.00055.
[32] F. Giustino, M. L. Cohen, and S. G. Louie, Phys. Rev. B **76**, 165108 (2007).
[33] P. Giannozzi *et al.*, J. Phys.-Condens. Mat. **21**, 395502 (2009).
[34] A. B. Migdal, Sov. Phys. JETP **34**, 996 (1958).
[35] G. M. Eliashberg, Sov. Phys. JETP **11**, 696 (1960).
[36] E. R. Margine and F. Giustino, Phys. Rev. B **87**, 024505 (2013).
[37] Coh S, Cohen M L and Louie S G, to be published.
[38] L. Boeri, M. Calandra, I. I. Mazin, O. V. Dolgov, and F. Mauri, Phys. Rev. B **82**, 020506 (2010).
[39] T. Bazhirov and M. L. Cohen, Phys. Rev. B **86**, 134517 (2012).
[40] T. Bazhirov and M. L. Cohen, J. Phys.-Condens. Mat. **25**, 105506 (2013).
[41] P. B. Allen and R. C. Dynes, Phys. Rev. B **12**, 905 (1975).
[42] Z. Li *et al.*, J. Phys.-Condens. Mat. **26**, 265002 (2014).
[43] R. Peng *et al.*, Nat Commun **5**, 5044 (2014).
[44] R. Peng *et al.*, Phys. Rev. Lett. **112**, 107001 (2014).
[45] C.-L. Song, Y.-L. Wang, Y.-P. Jiang, Z. Li, L. Wang, K. He, X. Chen, X.-C. Ma, and Q.-K. Xue, Phys. Rev. B **84**, 020503 (2011).
[46] C.-L. Song *et al.*, Science **332**, 1410 (2011).
[47] C.-L. Song, Y.-L. Wang, Y.-P. Jiang, Z. Li, L. Wang, K. He, X. Chen, J. E. Hoffman, X.-C. Ma, and Q.-K. Xue, Phys. Rev. Lett. **112**, 057002 (2014).
[48] R. Khasanov, M. Bendele, K. Conder, H. Keller, E. Pomjakushina, and V. Pomjakushin, New J. Phys. **12**, 073024 (2010).
[49] W. L. McMillan and J. M. Rowell, PRL **14**, 108 (1965).
[50] M. L. Cohen and V. Heine, Solid State Physics **24**, 37 (1970).
[51] L.-W. Wang and A. Zunger, Phys. Rev. B **51**, 17398 (1995).

Supplemental material for "Large electron-phonon interactions from FeSe phonons in a monolayer"

Sinisa Coh, Marvin L. Cohen, and Steven G. Louie
Department of Physics, University of California at Berkeley and Materials Sciences Division, Lawrence Berkeley National Laboratory, Berkeley, California 94720, USA
(Dated: July 10, 2015)

Technical details. For the semi-core iron pseudopotential used we obtain $A_c f(r) = (5.7\text{ Ry})e^{-r^2/(0.85\text{ bohr})^2}$. Near the center of the atom, the depth of this potential is only 6% of the local part of the pseudopotential. Throughout this work, we use GGA-PBE functionals with norm-conserving pseudopotentials that include semi-core electrons on Fe and Ti. We use a 180 Ry energy cutoff, 8x8x1 sampling of the electron Brillouin zone, and 4x4x1 sampling of the phonon Brillouin zone which we Wannier interpolate on a 40x40x1 grid. All conventions in the paper and the supplement are for the primitive unit cell with two Fe atoms per cell. Electron doping in our calculations equals 0.09 electrons per one Fe atom (as found in ARPES experiment).
Additional figures and one table can be found on the following pages.

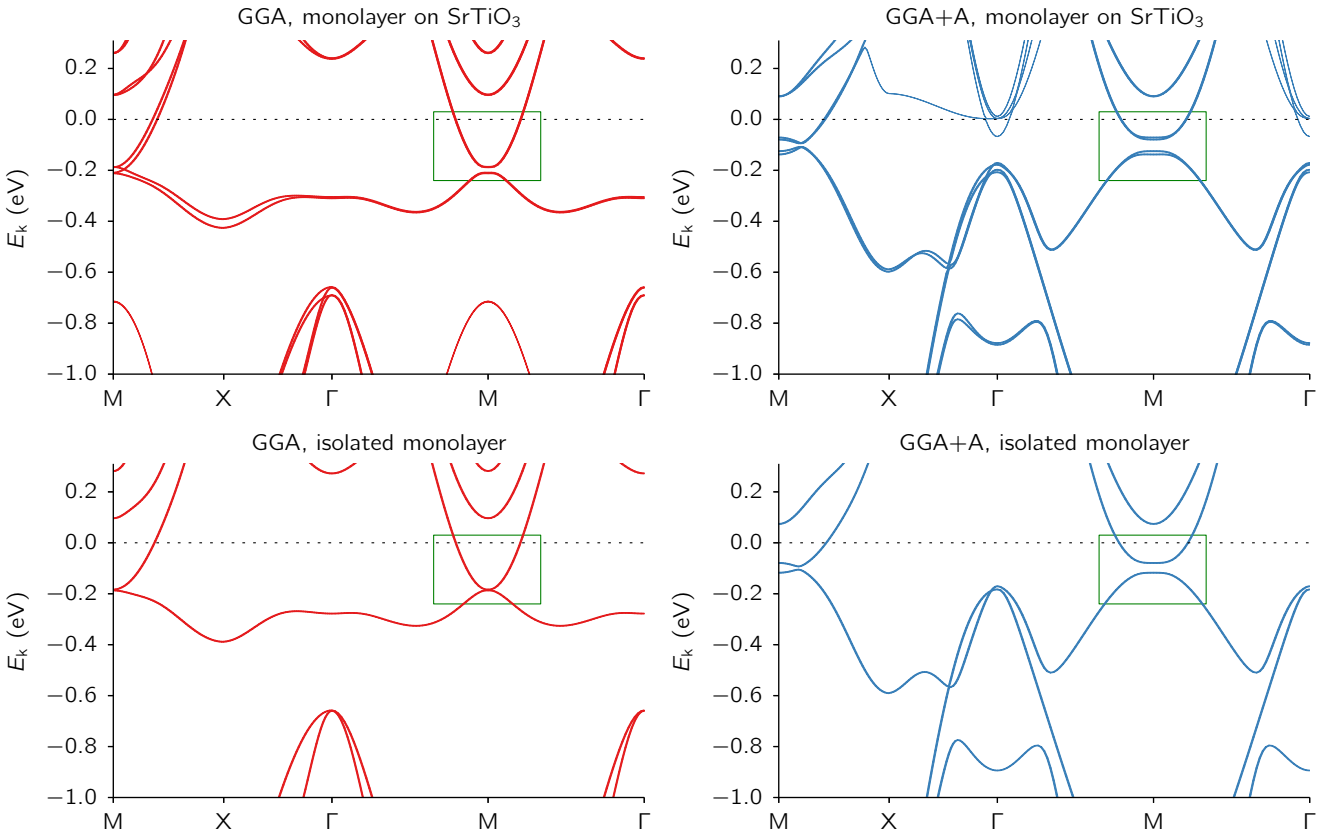

FIG. 1. Electronic band structure of FeSe monolayer on a path in momentum space calculated in GGA (red) and GGA+A (blue). Conventions are for the primitive unit cell with two Fe atoms per cell. Top two panels show the band structure of FeSe monolayer on a $SrTiO_3$ slab after a full structural relaxation. Bottom panels show the band structure when $SrTiO_3$ atoms are removed from the calculation while the FeSe monolayer atoms are kept at the same positions as in the full calculation. Thin lines in the topmost panels correspond to the electronic bands localized on the $SrTiO_3$ slab. Thick lines are states localized on FeSe. Green squares indicate region of the band structure plot that is shown in Fig. 1 in the main text. Computational unit cell used in our calculation consists of a $SrTiO_3$ slab covered with FeSe monolayer on each end, so that both ends of $SrTiO_3$ are passivated in the same manner. Hybridization between these two monolayers of FeSe causes small splitting seen on the M-X line at 0.2 eV below the Fermi level in the top-left panel, and at the bottom of the M pocket in the top right panel. This hybridization splitting disappears in the lower panels because in that case computational cell contains only one FeSe monolayer.

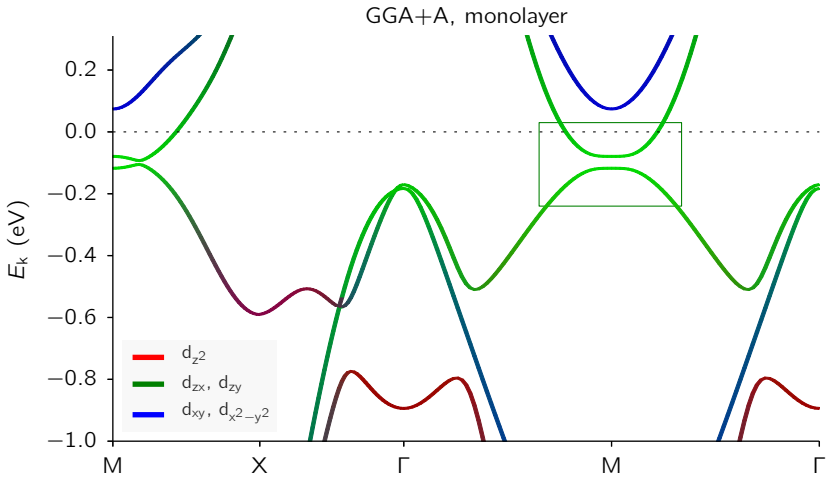

FIG. 2. The d-character of the electron wavefunction in the FeSe monolayer. Line segments colored red corresponds to the d_{z^2} states, green to the d_{zx} and d_{zy}, and blue to d_{xy} and $d_{x^2-y^2}$ states. Everything in the figure except for the coloring scheme is the same as in the lower right panel of Fig. 1 in the supplement.

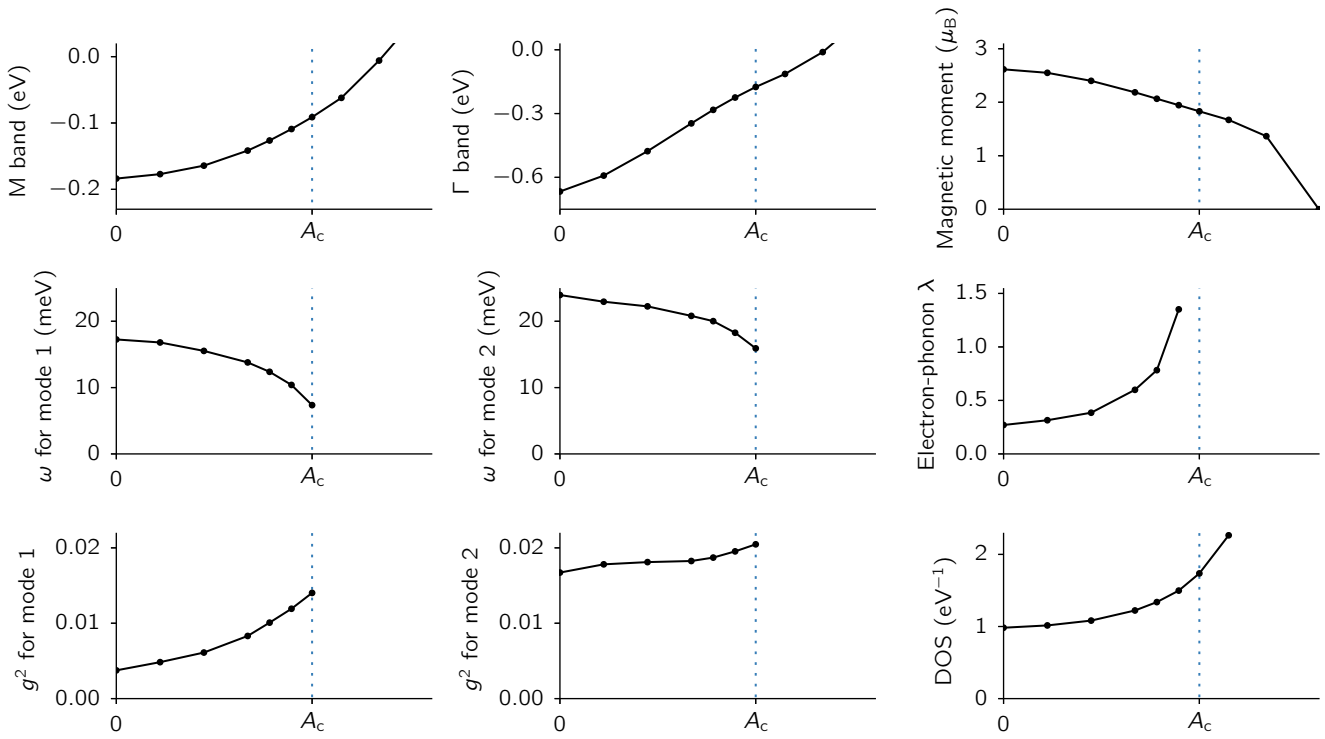

FIG. 3. Dependence of nine properties of an isolated FeSe monolayer on the value of parameter A in the GGA+A approach: bottom of the M pocket (occupied bandwidth, E_M), top of the Γ pocket (E_Γ), magnetic moment on the iron atom, frequency of phonons (ω) with dominant electron-phonon coupling (modes 1 and 2 discussed in the main text), total electron-phonon coupling strength λ, electron phonon matrix element squared (g^2) for dominant modes 1 and 2, and density of states at the Fermi level. Dashed blue line shows $A = A_c$ case discussed in the main text. Regular GGA result (without A) corresponds to $A = 0$. Here the $SrTiO_3$ substrate was not explicitly included in the calculation. Instead, the FeSe monolayer was structurally relaxed with the in-plane lattice constant equal to that of $SrTiO_3$. Phonon eigendisplacements of modes 1 and 2 are taken from $A = 0.9A_c$ calculation and then used for all values of A for consistency.

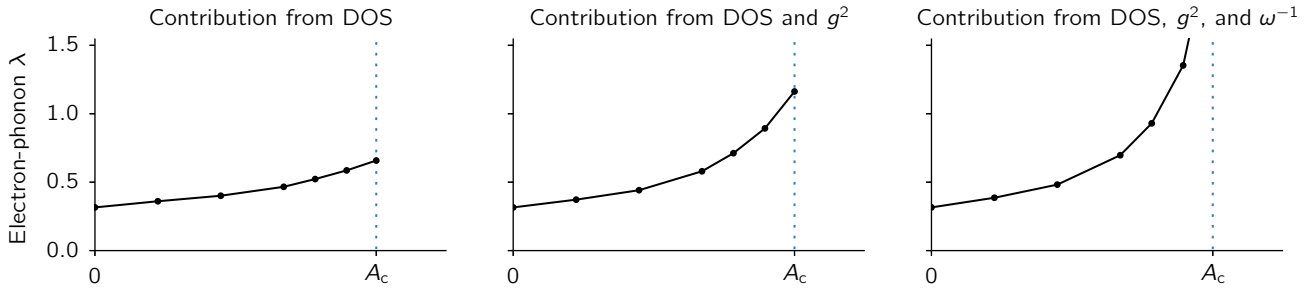

FIG. 4. Contribution to lambda in the case of an isolated FeSe monolayer. We show contributions of density of state (DOS) increase, electron-phonon matrix element squared (g^2) increase, and phonon frequency softening (ω^{-1}) to the increase in λ as a function of parameter A. Critical behavior of λ at A_c originates from phonon softening at $A = A_c$ since these calculations do not include $SrTiO_3$ substrate. As we show in Table. I and Fig. 5, critical behavior is removed once substrate is included in the calculation. Here we used calculated contribution of phonons 1 and 2 to λ at $0.9A_c$ and isolated dependence of λ on DOS, g^2, and ω^{-1} using the following simplified expression for $\lambda \sim \mathrm{DOS} \times g^2 \times \omega^{-1}$.

TABLE I. Electron-phonon matrix elements (g^2 in atomic units) and phonon frequencies (in meV) of the dominating phonon modes (modes 1 and 2, see main text) at $A = 0.9A_c$ calculation without a substrate, and $A = A_c$ with a substrate. For computational convenience, we first calculate phonon eigendisplacements with $A = 0.9A_c$ and no substrate, and then use those same eigenvectors in the $A = A_c$ calculation explicitly including the $SrTiO_3$ substrate.

	Dominant phonon 1		Dominant phonon 2	
	g^2 (au)	ω (meV)	g^2 (au)	ω (meV)
Isolated FeSe with $A = 0.9A_c$	0.012	10	0.020	18
FeSe on $SrTiO_3$ substrate with $A = A_c$	0.010	7	0.019	17

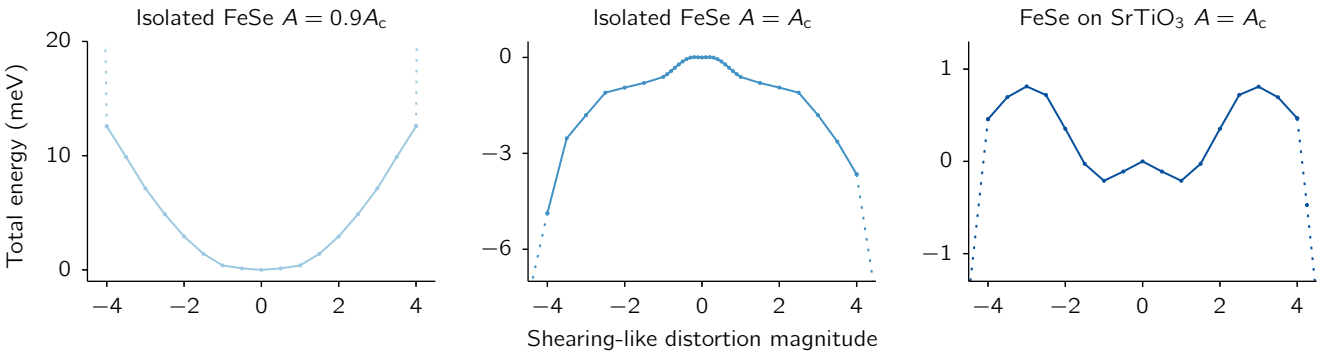

FIG. 5. Total energy per unit cell (Fe_2Se_2 formula unit) as a function of shearing-like distortion for isolated FeSe with $A = 0.9A_c$ and $A = A_c$, as well as FeSe on $SrTiO_3$ with $A = A_c$. Presence of $SrTiO_3$ stabilizes the shearing-like distortion present in the isolated FeSe monolayer at A_c. Only a small amount of shearing distortion is present in the fully relaxed ground state of FeSe on $SrTiO_3$ (corresponding to ± 1 on the horizontal scale). This distortion is responsible for a gap (δE_M) at the M point shown in Fig. 1 of the main text. If shearing distortion is artificially increased beyond ± 4 (dashed lines), the gap δE_M increases and the system undergoes a metal-insulator transition in all three cases. Therefore, the energy landscape for a shearing distortion in FeSe monolayer is driven by a gap opening of a small-area electron pocket at the M point.

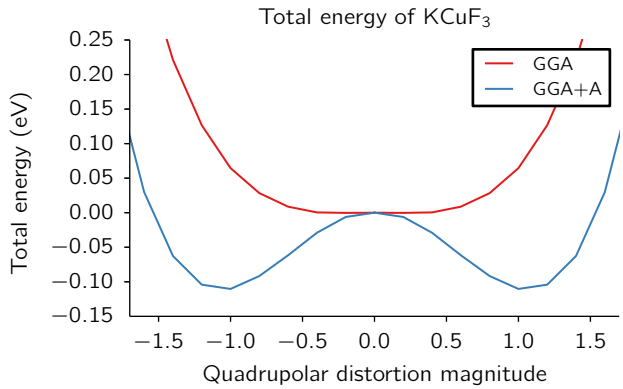

FIG. 6. Total energy of paramagnetic $KCuF_3$ (per one formula unit) as a function of fluorine quadrupolar distortion within GGA (red) and GGA+A (blue). Ground state within GGA shows no preference for this distortion unlike GGA+A (horizontal scale is chosen so that ± 1 corresponds to the experimental value of the distortion magnitude). Similar preference for fluorine quadrupolar distortion was found by including Hubbard +U and +J term in Ref. [1].

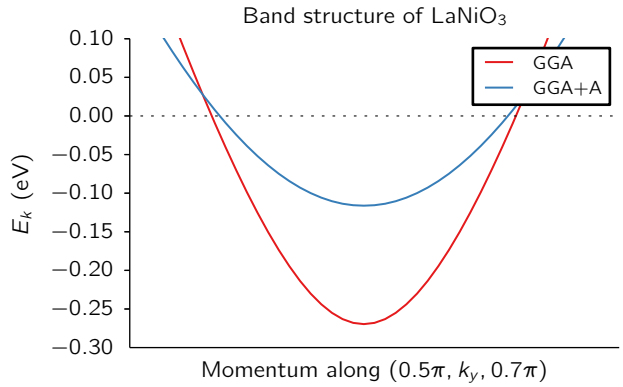

FIG. 7. Band structure of $LaNiO_3$ along the $(0.5\pi, k_y, 0.7\pi)$ line shows a large mass renormalization once +A term is included (blue versus red curve). This is consistent with the experimental finding from Ref. [2] (ARPES data in Ref. [2] is shown along the same path in the momentum space).

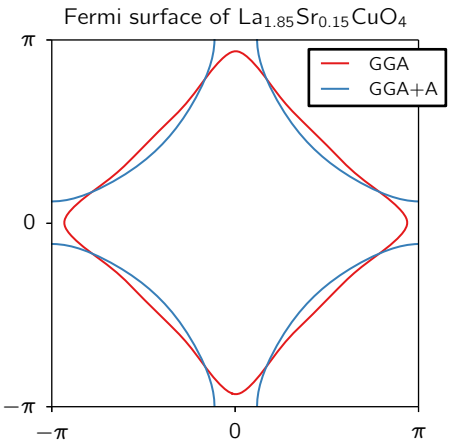

FIG. 8. Fermi surface of optimally doped $La_{1.85}Sr_{0.15}CuO_4$ shows different topology in GGA (red) and GGA+A (blue), with the latter consistent with experimental findings in Ref. [3].

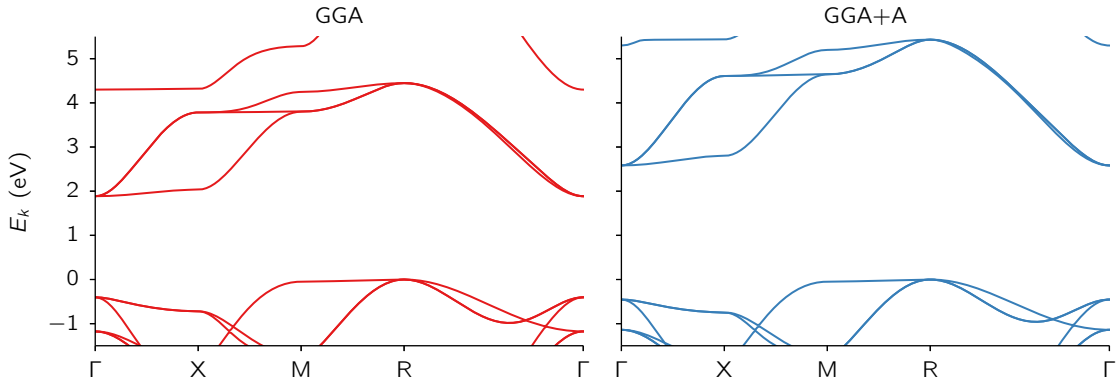

FIG. 9. Band structure of $SrTiO_3$ within GGA (red) and GGA+A (blue). Direct and indirect band gaps in GGA (2.3 and 1.9 eV) are increased once the +A term is included (3.0 and 2.6 eV) in better agreement with the experimental data from Ref. [4].

[1] A. I. Liechtenstein, V. I. Anisimov, and J. Zaanen, Phys. Rev. B **52**, 5467 (1995).
[2] P. D. C. King, H. I. Wei, Y. F. Nie, M. Uchida, C. Adamo, S. Zhu, X. He, I. Božović, D. G. Schlom, and K. M. Shen, Nat Nano **9**, 443 (2014).
[3] A. Ino, C. Kim, M. Nakamura, T. Yoshida, T. Mizokawa, A. Fujimori, Z.-X. Shen, T. Kakeshita, H. Eisaki, and S. Uchida, Phys. Rev. B **65**, 094504 (2002).
[4] K. van Benthem, C. Elsasser, and R. H. French, J. Appl. Phys. **90**, 6156 (2001).